Comparative Evaluation of NDWI, NDVI, MNDWI, AWEI and EWI for Sentinel-2 Shoreline Delineation in Klungkung, Indonesia: KDE-Valley vs Otsu Thresholding

Sakina Hasan[1*], Abd Rahman As-syakur[2], Xuan Truong Trinh[3], and Masahiko Nagai[4]

[1] Bachelor Student, Faculty of Marine and Fisheries, Udayana University, Indonesia

[2] Professor, Faculty of Marine and Fisheries, Udayana University, Indonesia

[3] Assistant Professor, Faculty of Engineering, Yamaguchi University, Japan

[4] Professor, Center for Research and Application of Remote Sensing, Yamaguchi University, Japan

* hasan.2213511062@student.unud.ac.id

Abstract

Shoreline detection is essential for coastal monitoring amid accelerating climate change and intensified human activities. This study examines the coastal area of Klungkung, which experiences recurrent erosion and abrasion. We evaluated six spectral indices-NDVI, NDWI, Modified NDWI (MNDWI), Automated Water Extraction Index-shadow (AWEI-SH), AWEI-non-shadow (AWEI-NSH), and the Enhanced Water Index (EWI)-using Sentinel-2 imagery to delineate the shoreline. Two methods were used to distinguish the shoreline from the sea: automatic thresholding using Otsu method and applying a kernel density estimation (KDE) valley approach with manually selected training samples. Shorelines from each index were validated against the Last Vegetation Line (LVL) surveyed with a Garmin GPS, and mean distances to the LVL were compared. Results (mean distance error, meters) show that NDWI (6.26 m) and NDVI (6.45 m) outperformed MNDWI (10.50 m) and EWI (9.70 m). For NDWI, KDE-based thresholding yielded higher accuracy than the Otsu method (6.26 m vs. 10.23 m). The lower performance of MNDWI and EWI likely reflects the use of 20-m Sentinel-2 bands, which reduced delineation precision. NDVI performed on par with NDWI, possibly because the vegetation line defines the validation shoreline. In this setting, NDWI and NDVI, particularly when paired with appropriate thresholding, provide high-accuracy shoreline detection. Future work should test higher-resolution sensors and extend the approach to region-wide shoreline monitoring.

Keywords: Coastal erosion, Last Vegetation Line (LVL), Field validation (GPS), Water indices, Shoreline Monitoring

Introduction

The shoreline represents the boundary between land and the sea surface, characterized by highly dynamic properties (Dey et al., 2024). Globally, the total length of shorelines is estimated at approximately 504,000 km, with Indonesia ranking second after Canada, having a shoreline length of 95,161 km. More than 50% of the world's population resides within a 100 km radius of the sea (Arianto, 2020; Toure et al., 2019). According to Parenta (2021) and Aryastana et al. (2016), natural factors such as waves, currents, and tides play a crucial role in the processes of erosion and accretion, which drive shoreline change. Hydrological, geological, climatic, and vegetation factors also contribute to shoreline dynamics. Beyond natural drivers, human activities significantly influence shoreline change through coastal development, land reclamation, and mining activities (Hidayah et al., 2018). Such anthropogenic impacts can lead to erosion and accretion, often resulting from land clearance and the extraction of mineral resources in coastal zones, which may alter shoreline conditions (Safitri et al., 2019).

In Indonesia, one of the regions experiencing notable shoreline change is Klungkung Regency, which has a total shoreline length of approximately 90–113 km, including both mainland and island coasts (Singa et al., 2023; Diasa et al., 2024). Around 44% of this shoreline, or about 26 km, has undergone erosion, with rates between 0.058 m/year and 1.846 m/year, while accretion rates range from 0.055 m/year to 1.084 m/year (Singa et al., 2023). These changes have resulted in the degradation of temple structures and the loss of coastal stalls that once served as tourist facilities, highlighting the urgent need for effective shoreline monitoring and management.

To develop effective shoreline detection methods, various approaches can be applied, including bathymetric mapping using acoustic waves (sonar), land surveys based on landmarks, Global Positioning System (GPS) measurements, terrestrial Light Detection and Ranging (LiDAR), as well as remote sensing using satellite imagery (Toure et al., 2019). A number of previous studies have employed remote sensing techniques for this purpose. For instance, Esendağlı et al. (2022) evaluated the performance of five automated indices derived from Landsat 9 imagery, namely the Normalized Difference Vegetation Index (NDVI), Normalized Difference Water Index (NDWI), Automated Water Extraction Index (AWEI), Water Ratio Index (WRI), and Normalized Difference Moisture Index (NDMI). Their results indicated that AWEI achieved the highest accuracy, followed by NDWI, WRI, NDMI, and NDVI. Furthermore, AWEI demonstrated consistent performance across various land cover types, while NDVI showed improved accuracy in densely vegetated areas. Another study by Hastuti

et al. (2024) employed Sentinel-2 imagery to evaluate five water indices, including NDVI, NDWI, Modified Normalized Difference Water Index (MNDWI), WRI, and AWEI. This study found that MNDWI was the most accurate in detecting water bodies, whereas NDVI performed better in vegetated areas. However, both studies lacked in-situ validation data and only compared the index-based results with high-resolution satellite imagery from PlanetScope and Google Earth. In addition, both relied on the commonly used Otsu thresholding method, without considering alternative approaches such as Kernel Density Estimation (KDE) for threshold determination.

The Otsu method, introduced by Nobuyuki Otsu (1979), is an image segmentation technique that automatically determines the threshold by maximizing between-class variance. This method is effective for bimodal histograms without requiring prior parameters, but it is less optimal when applied to noisy or multimodal histograms (Korneev et al., 2022). In remote sensing, particularly for shoreline extraction, Otsu is often combined with spectral indices such as NDWI or MNDWI to improve land–water separation accuracy (Tang et al., 2022). As an alternative, Kernel Density Estimation (KDE) is used to smooth intensity distributions so that peaks and valleys become more distinct. The KDE-valley approach selects the valley between peaks as the threshold. This method is more robust to noise and can be extended to multi-class segmentation, although it requires appropriate bandwidth selection and higher computational costs compared to Otsu (Botev et al., 2010; Korneev et al., 2022).

This study aims to evaluate the accuracy of five water indices in remote sensing, namely NDVI, NDWI, MNDWI, AWEI, and EWI, for shoreline detection in Klungkung Regency. The evaluation is conducted by comparing shoreline extraction results from satellite imagery with field validation data (ground truth) in the form of the last vegetation line obtained through GPS surveys. Furthermore, the study compares the performance of two thresholding methods, KDE-valley and Otsu, in the shoreline delineation process. The analysis is expected to identify the most representative and effective water index for shoreline mapping in the study area. The scope of this research is limited to the comparison of water indices and does not address coastal oceanographic factors such as tides, waves, currents, or winds, which may dynamically influence shoreline position.

Methodology

a. Study Area

The research was conducted in Klungkung Regency, Bali Province, spanning the

coastal zone from Tegal Besar Beach (Negari Village) to Goa Lawah Beach (Pesinggahan Village), adjacent to Karangasem Regency (Figure 1). Field data for validation were collected on February 9, 10, 15, and 16, 2025, between 09:00 and 17:00 Central Indonesia Time (CIT).

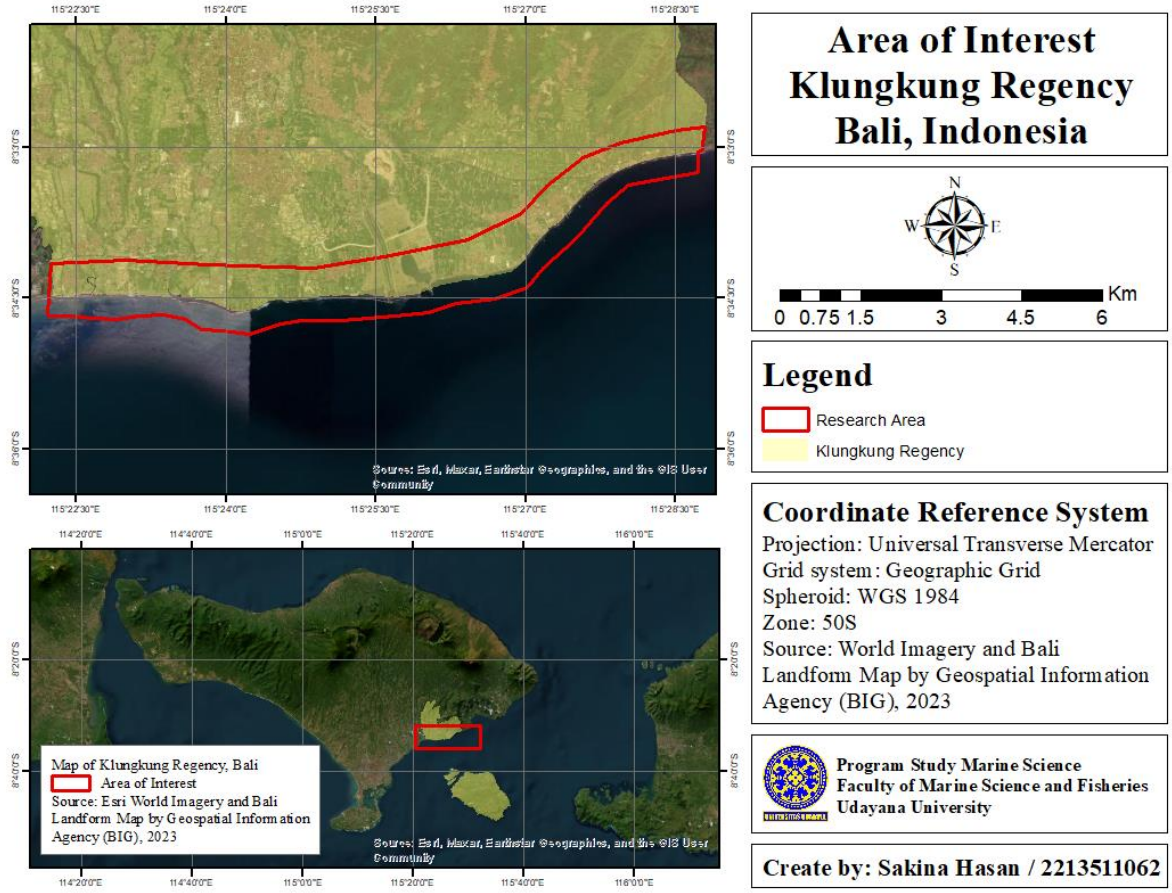

Figure 1: Area of Interest

b. Data Collection

Primary data were collected through field surveys conducted from 9 to 16 February 2025, between 09:00 and 17:00 local time (WITA). Observation points were established along the last vegetation line at 50 m intervals. Five coordinates were recorded at each point, consisting of one primary coordinate and four repeated measurements. Priority was given to overlapping coordinates; if no overlap occurred, the coordinate closest to the 50 m interval from adjacent points was selected (Figure 2).

Secondary data consisted of Sentinel-2 Level-2A imagery, which was chosen as the primary dataset due to its 10–20 m spatial resolution, broad spectral coverage, 5-day revisit cycle, and free accessibility, making it suitable for coastal monitoring (Li & Roy, 2017;

Pahlevan et al., 2017). The imagery was accessed via Google Earth Engine (GEE) to facilitate cloud-free image selection and downloading. A scene acquired on 25 February 2025 was selected, as its cloud cover did not obscure the main coastal area of interest.

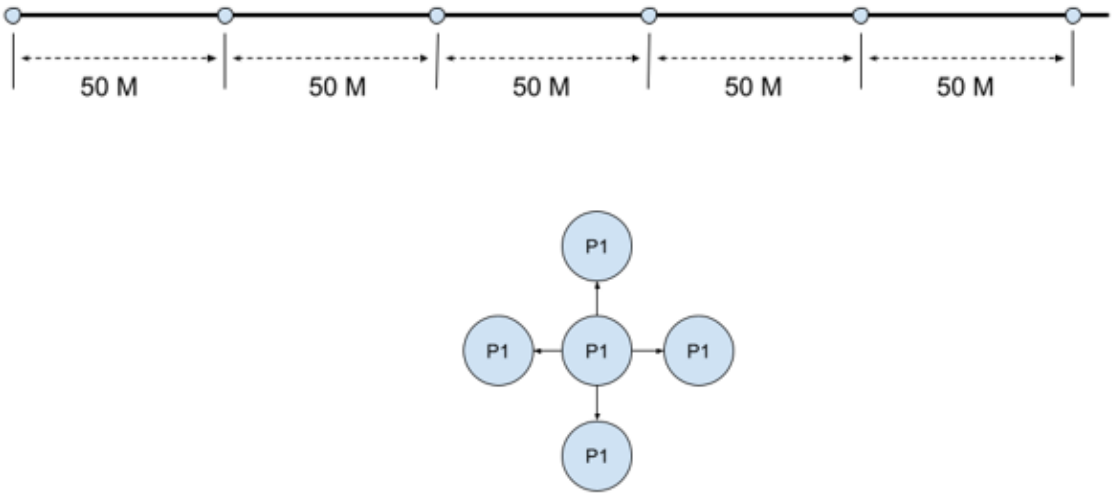

Figure 2: Primary Data Collection Method

Sentinel-2 satellite imagery was the secondary data source and was accessed via Google Earth Engine (GEE), facilitating image selection, acquisition of cloud-free imagery, and data download. The data collection involved delineating the study area using geographic coordinates, selecting cloud-free images to ensure unobstructed analysis, and performing quality checks, including radiometric correction. Level-2A Sentinel-2 images underwent atmospheric correction and were used for water and vegetation index analysis.

Imagery dates were selected to correspond with field conditions. The 25 February 2025 image, with 33% cloud cover, was chosen over the 15 February image (34% cloud cover) because cloud positions on the earlier image obscured key coastal areas. Field data (ground truth) were collected concurrently to provide direct information on coastal water and vegetation conditions and to validate that the satellite-derived indices accurately represent real-world conditions.

c. Image Processing

i. Calculation of Remote Sensing Indices

In the water body and vegetation extraction stage, several spectral-based indices derived from satellite imagery were calculated, including the Normalized Difference Vegetation Index (NDVI), Normalized Difference Water Index (NDWI), Modified NDWI (MNDWI), Automated Water Extraction Index (AWEI), and Enhanced Water

Index (EWI).

The NDVI, developed by Rouse et al. (1973), utilizes the difference in reflectance between the near-infrared (NIR) and red (R) bands to estimate vegetation biomass and photosynthetic activity. This index has been widely used because it effectively represents vegetation greenness and overall health (Andini et al., 2018).

$$\text{NDVI} = \frac{(\boldsymbol{NIR-RED})}{(\boldsymbol{NIR+RED})} \quad (1)$$

The Normalized Difference Water Index (NDWI), introduced by McFeeters (1996), is designed to detect the presence of water bodies by utilizing the difference in reflectance between the green (G) and near-infrared (NIR) bands. Positive index values typically indicate water bodies, while negative values represent vegetation or land surfaces. This index is often selected because of its simplicity, ease of application, and extensive use in remote sensing studies (Andini et al., 2018).

$$\text{NDWI} = \frac{(Green-NIR)}{(Green+NIR)} \quad (2)$$

The Modified Normalized Difference Water Index (MNDWI), developed by Xu (2006), replaces the Near-Infrared (NIR) band with the Short-Wave Infrared (SWIR) band. This modification enhances the index's ability to distinguish water bodies from vegetation and built-up areas. According to Du et al. (2016), MNDWI outperforms NDWI in regions characterized by dense vegetation cover or highly urbanized environments. Therefore, MNDWI is considered an appropriate choice to minimize water body misclassification in study areas with complex land cover conditions.

$$\text{MNDWI} = \frac{(Green-SWIR)}{(Green+SWIR)} \quad (3)$$

The Automated Water Extraction Index (AWEI) was developed to reduce misclassification errors caused by shadows or dark surfaces often mistakenly identified as water (Li & Gong, 2016). This index combines several spectral bands, including green, near-infrared (NIR), shortwave infrared 1 (SWIR1), and shortwave infrared 2 (SWIR2), to improve classification accuracy. Two versions of AWEI have been proposed to address different environmental conditions: one for shadowed areas (AWEI-sh) and another for non-shadowed areas (AWEI-nsh) (Feyisa et al., 2014). The AWEI-sh version is specifically designed to handle regions affected by shadows, such as mountainous or urban areas, by reducing the likelihood of shaded terrain or dark surfaces being

misclassified as water. In contrast, the AWEI-nsh version performs better in flat or open regions with minimal shadow interference, where lighting conditions are more uniform (Feyisa, et al. 2014).

$$\text{AWEI}_{nsh} = 4 \times (Green - SWIR) - (0.25 \times NIR + 2.75 \times SWIR) \quad (4)$$

$$\text{AWEI}_{sh} = Blue + 2.5 \times Green - 1.5 \times (NIR + SWIR) - 0.25 \times SWIR \quad (5)$$

The Enhanced Water Index (EWI) is an advancement of normalized water indices that combines the blue (B), green (G), near-infrared (NIR), and shortwave infrared (SWIR) bands, as formulated by Yan et al. (2007) and later discussed by Liu et al. (2023). By incorporating a broader range of spectral bands, EWI enhances the separation between water bodies and non-water features, particularly in areas with high spectral mixing. In this study, EWI was employed to provide a more comprehensive approach to capturing spectral variations of water.

$$\text{EWI} = \frac{Green - NIR - SWIR}{Green + NIR + SWIR} \quad (6)$$

The use of these five indices in this study was intended to obtain more accurate water body extraction results while also comparing the performance of each method within the study area. This approach allows for identifying the most suitable index to support further spatial analyses.

ii. Image thresholding

At the image thresholding stage, vegetation and non-vegetation were separated using two methods. The first method was Otsu thresholding, which automatically determines the optimal threshold value based on the pixel intensity histogram. The second method was a sample point–based Kernel Density Estimation (KDE) approach, in which random sample points were selected from each object class (water, sand, grass, and trees) to construct the pixel probability distribution. The threshold value was then derived from the KDE distribution peaks, allowing for more precise object separation and providing more substantial support for segmentation validation.

iii. Smoothing

After the thresholding stage, a smoothing process was carried out to reduce residual disturbances or noise in the satellite image segmentation results. In this study, smoothing was performed using the Sieve and Fill No Data tools available in QGIS (Hassan et al., 2018). The Sieve tool was applied to remove small areas that were inconsistent with their

surrounding class, such as single pixels or small pixel clusters that were misclassified. This process was conducted by defining a minimum area threshold, so that all areas smaller than this threshold were merged into the largest neighbouring class. As a result, the boundary between land and water became clearer, and the contours of the extracted objects appeared more consistent. Subsequently, the Fill No Data tool was used to fill empty pixels (No Data) that might appear after the Sieve process or during segmentation. These empty pixels were replaced with values from their surrounding pixels, ensuring that the segmented areas were more complete and homogeneous.

iv. Shoreline Extraction

The shoreline extraction stage aimed to delineate the boundary between pixel classes in the satellite imagery after thresholding and smoothing, thereby producing a precise and clear line representing the transition between areas (Hassan et al., 2018). Pixels located along the boundaries between classes were used as the basis for line generation. The segmented raster image was then converted into polygons using the *Raster to Polygon* tool in QGIS, which represented the boundaries of each class. These polygons were subsequently converted into vector lines using the *Polygon to Line* tool, ensuring that the extracted shoreline followed the shape of the area transitions in the imagery with both smoothness and precision.

d. Accuracy Validation

Accuracy validation in this study was conducted to assess the degree of closeness between the measurement results and the reference values, using three indicators: Mean Absolute Error (MAE), Mean Squared Error (MSE), and Root Mean Squared Error (RMSE).

i. Mean Absolute Error (MAE)

The Mean Absolute Error (MAE) is used to measure the average magnitude of deviation from the reference values, thereby providing an estimate of the average error expressed in meters (Hodson, 2022).

$$\boldsymbol{MAE} = \frac{\mathbf{1}}{\boldsymbol{n}}\sum_{\boldsymbol{i=1}}^{\boldsymbol{n}} |\boldsymbol{Yi} - \widehat{\boldsymbol{Y}}\boldsymbol{i}| \qquad (1)$$

ii. Mean Squared Error

The Mean Squared Error (MSE) is employed to evaluate the impact of larger errors, as each deviation is squared, thereby assigning greater weight to data points with high variance (Chicco et al., 2022).

$$MSE = \frac{1}{n}\sum_{i=1}^{n}(Yi - \hat{Y}i)^2 \quad (2)$$

iii. Root Mean Squared Error

The Root Mean Squared Error (RMSE), as the square root of the MSE, restores the error to the original units of the data while still emphasizing larger deviations, making it a comprehensive indicator for evaluating overall data accuracy (Amansyah et al., 2024).

$$RMSE = \sqrt{\frac{1}{n}\sum_{i=1}^{n}(Yi - \hat{Y}i)^2} \quad (3)$$

.

Results and Discussion

a. Performance of Remote Sensing Indices (NDVI, NDWI, MNDWI, AWEI, EWI) in Shoreline Extraction

The results of the analysis demonstrate that each index has its own strengths and limitations in delineating the boundary between land and water in coastal zones. In this study, the Automated Water Extraction Index (AWEI) proved to be particularly effective in urban and settlement areas. Built-up regions generally contain many dark materials, such as rooftops, roads, and shadows, which often lead to misclassification when using other water indices. Both AWEI-nsh and AWEI-sh effectively suppressed errors caused by dark surfaces and shadows, thereby producing a more reliable separation between water and non-water pixels compared to other indices. As shown in Figure 5, AWEI combined with automatic thresholding methods such as Otsu and KDE Valley yielded consistent shoreline detection results in built-up and river mouth areas (Feyisa et al., 2014).

The Normalized Difference Vegetation Index (NDVI) showed the best performance in areas dominated by vegetation, regardless of whether Otsu or KDE Valley thresholding was applied. NDVI is designed to distinguish vegetation from non-vegetation, with high values indicating healthy vegetation and low values representing non-vegetative surfaces such as sand or water (McFeeters, 1996). Consequently, NDVI provides sharp contrast along vegetation–water or vegetation–sand boundaries, thereby facilitating shoreline delineation in vegetated ecosystems such as coastal shrubs and mangroves.

The Modified NDWI (MNDWI) and other indices utilizing the SWIR band, such as the Enhanced Water Index (EWI), exhibited different behavior compared to the classical NDWI. Replacing the NIR band with SWIR improves MNDWI's ability to suppress interference from built-up land cover (Xu, 2006). However, on sandy coastlines, both

MNDWI and EWI frequently classify dry or thin sand layers as non-water. As a result, shorelines extracted from these indices tend to shift further seaward compared to indices that classify wet sand as water. This finding is consistent with previous comparative studies of water indices in coastal regions (Zhou et al., 2023).

In contrast, the classical NDWI (green vs. NIR) often includes wet sand or tidal zones within the water class due to its sensitivity to surface moisture (McFeeters, 1996). These differences in sensitivity among indices explain the variability in shoreline positions, with some indices shifting more seaward and others landward. Thus, the choice of spectral band combinations is a critical factor in determining how surfaces such as dry and wet sand, mud, vegetation, and built-up areas are classified (Xu, 2006).

The Otsu thresholding method offers the advantage of automation, reducing the need for manual intervention, and generally performs well on single images. However, Otsu is limited when index value distributions overlap or exhibit multimodality, as in cases involving mixtures of water, wet sand, dry sand, vegetation, and built-up surfaces (Tang et al., 2022). To address this limitation, the KDE Valley method was applied as an alternative, allowing threshold selection based on data distribution and representative ground-truth points. As illustrated in Figure 3, the KDE Valley method provided more flexible threshold determination by considering the shape of the histogram and data clustering, while Figure 4 shows that Otsu often produced sharper, though sometimes less adaptive, threshold boundaries.

In this study, the application of KDE Valley to NDVI did not produce significant differences compared to Otsu, since NDVI consistently distinguishes vegetation from non-vegetation. For NDWI and AWEI, both methods produced relatively similar shorelines, though minor discrepancies were observed: with KDE Valley, some buildings were classified as non-vegetation, whereas Otsu classified them as non-water. More substantial differences were observed for MNDWI and EWI. At river mouths, Otsu tended to classify sand as non-water, while KDE Valley in the same areas sometimes classified the sand as vegetation or even water. These findings, as visualized in Figure 5, highlight that the choice of thresholding method can significantly influence the final results, particularly in complex transitional environments such as river mouth zones.

Figure 3: KDE Valley Results Image

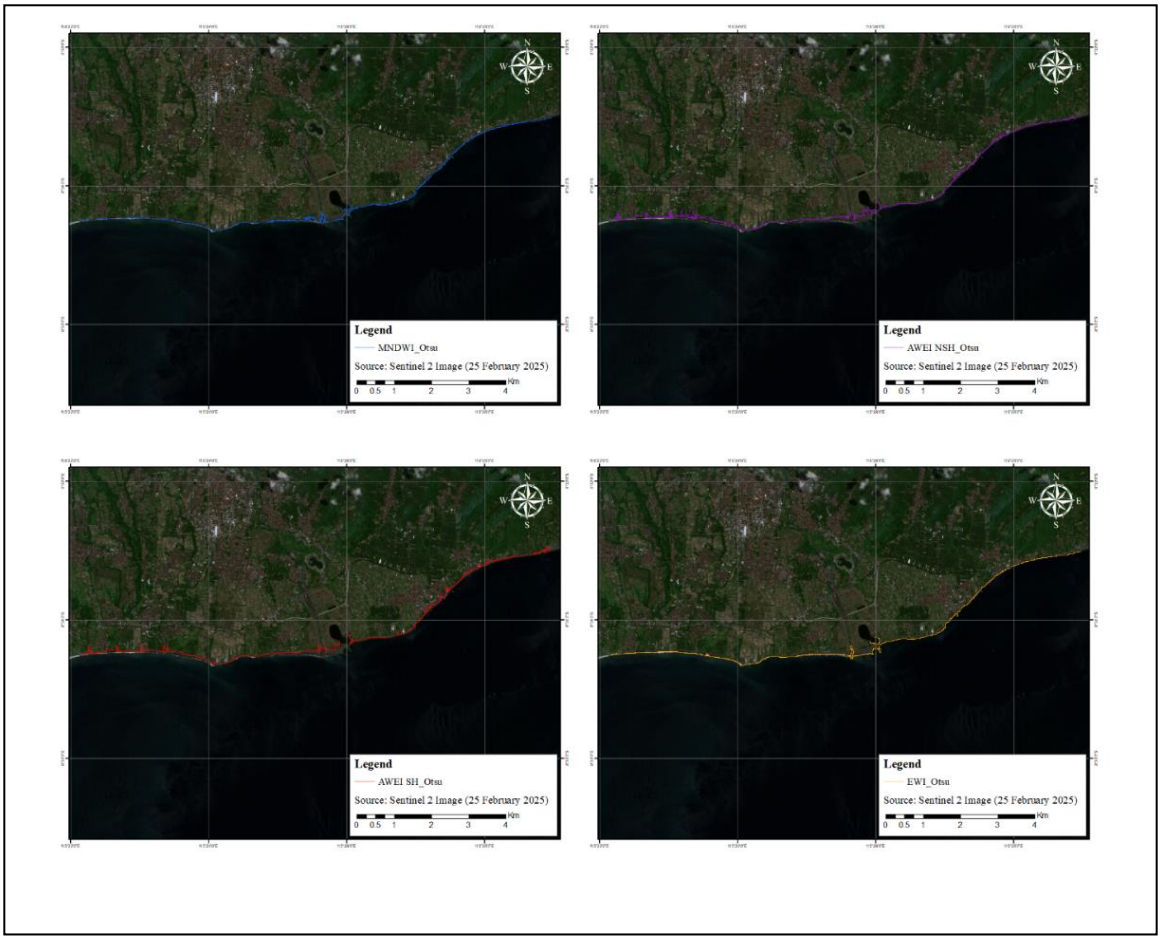

Figure 4: Otsu Results Image

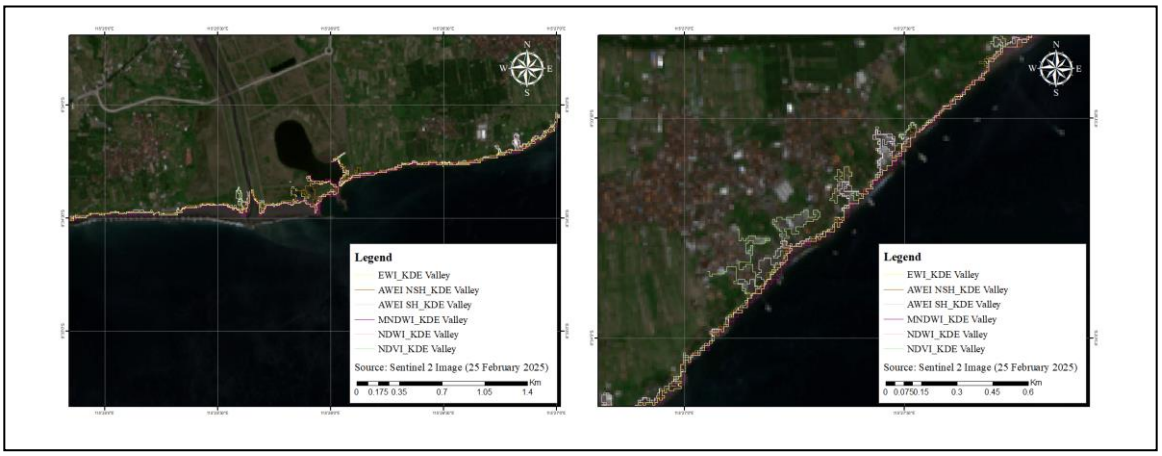

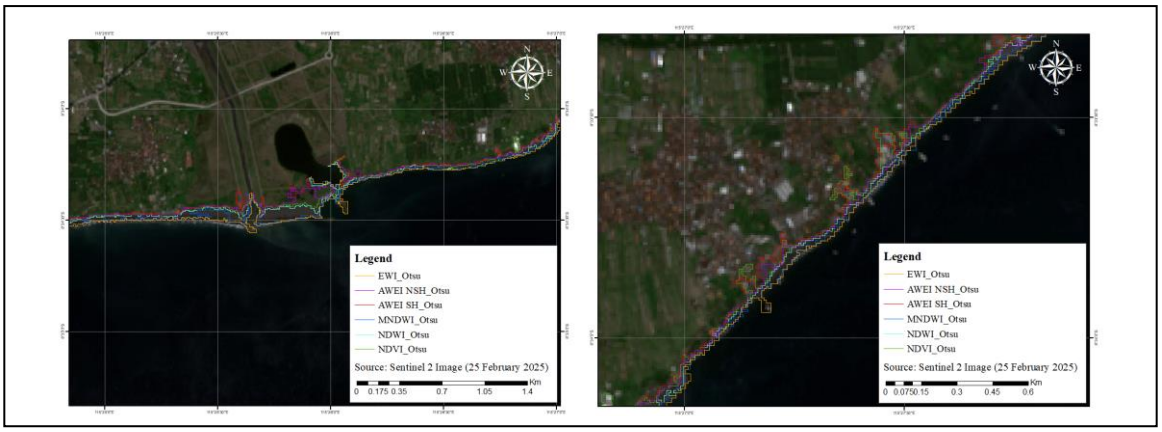

Figure 5: River and Urban area using KDE Valley and Otsu

b. Comparison of Thresholding Methods (Otsu vs. KDE-Valley) for Delineation Accuracy

Table 1: Accuracy Validation Result

No	Index	Otsu			KDE		
		MAE (m)	MSE (m^2)	RMSE (m)	MAE (m)	MSE (m^2)	RMSE (m)
1	NDVI	6.52	142.84	11.95	7.24	181.41	13.47
2	NDWI	10.53	169.25	13.01	6.39	120.31	10.97
3	MNDWI	22.99	795.29	28.20	11.02	220.12	14.84
4	AWEI SH	9.32	297.39	17.25	8.02	198.16	14.08
5	AWEI NSH	13.73	825.33	28.73	11.25	532.89	23.08
6	EWI	29.61	1234.60	35.14	9.81	173.06	13.16

Based on the comparison between the Otsu and KDE Valley methods, variations in performance were observed across the three accuracy evaluation parameters (MAE, MSE, and RMSE) for each remote sensing index. The Mean Absolute Error (MAE) results indicate that the KDE method generally produced lower errors than Otsu, demonstrating better adaptability to complex data distributions. For instance, NDWI improved from 10.53 m (Otsu) to 6.39 m (KDE), MNDWI decreased from 22.99 m to 11.02 m, and EWI showed a substantial reduction from 29.61 m to 9.81 m. These results suggest that the density-based thresholding approach (KDE Valley) is more effective at handling multimodal or skewed pixel histogram distributions in coastal imagery, compared to the global thresholding method of Otsu, which assumes a simple bimodal distribution (Otsu, 1979).

The ground-truth reference used in this study was the last vegetation line, representing the boundary between vegetated and non-vegetated areas. This strengthens the applicability

of the KDE approach, as vegetation transitions typically exhibit gradual spectral changes rather than sharp separations. The improved accuracy (lower MAE values) under the KDE method supports this reasoning, indicating that KDE can better adapt to smooth spectral transitions compared to Otsu, which often struggles with non-bimodal distributions (Liu et al., 2023; Zhou et al., 2023).

Both AWEI-SH and AWEI-NSH showed relatively stable performance across both thresholding methods, with only moderate improvements under KDE. AWEI-SH decreased from 9.32 m (Otsu) to 8.02 m (KDE), while AWEI-NSH decreased from 13.73 m to 11.25 m. These indices consistently demonstrated low MSE and RMSE values, confirming the robustness of AWEI in minimizing the influence of shadows and dark surfaces in coastal environments. This finding aligns with Feyisa et al. (2014), who emphasized the capability of AWEI to reduce misclassification errors in shaded or complex illumination conditions.

In contrast, NDVI exhibited a slight increase in error when using the KDE method, with MAE rising from 6.52 m (Otsu) to 7.24 m (KDE). This can be explained by the nature of NDVI, which is specifically designed to distinguish vegetation from non-vegetation and thus presents a clearly bimodal distribution. In such cases, the Otsu method is sufficient for effective segmentation, as its global thresholding assumption fits well with the distinct separation between vegetation and non-vegetation classes (Clinton, 2017). The KDE method, which introduces more flexibility in threshold determination, may therefore add unnecessary complexity when the data distribution is already well defined (Li & Chen, 2021).

Conclusion and Recommendation

a. Conclusion

Based on the comparison results, the KDE method generally demonstrated better performance than Otsu, particularly for NDWI, MNDWI, AWEI-SH, AWEI-NSH, and EWI. The significant reduction in MAE values across most indices confirms that KDE is more adaptive in handling complex histogram distributions. This finding is especially relevant since the ground truth data used in this study were the last vegetation line, where vegetation boundaries often lack sharp contrasts. Specifically, for NDWI, the decrease in MAE from 10.53 (Otsu) to 6.39 (KDE) highlights the sensitivity of this index in detecting water presence, enabling KDE to provide a more precise threshold for distinguishing vegetated and non-vegetated areas near water zones. Meanwhile, AWEI indices remained consistent and stable with both Otsu and KDE, demonstrating their effectiveness in

separating water from non-water as well as vegetation from non-vegetation. In contrast, NDVI displayed a different pattern, where KDE increased error rates. This indicates that for indices with relatively stable and bimodal distributions, such as NDVI, the Otsu method remains more appropriate than density-based thresholding.

b. Recommendation

First, the use of KDE is recommended for indices with complex spectral distributions, particularly NDWI, MNDWI, and EWI, as it can improve segmentation accuracy in areas with gradual spectral transitions such as coastal zones. Specifically for NDWI, KDE is highly recommended in studies focusing on the interaction between vegetation and water bodies, as its significant accuracy improvement demonstrates strong potential for delineating both water boundaries and the last vegetation line. Second, for indices with inherently clear bimodal distributions, such as NDVI, the Otsu method remains sufficient without the need for additional complexity from KDE. Third, AWEI can be considered a reliable alternative for water body extraction, particularly in shadowed areas, due to its consistent performance under both methods. For future research, it is recommended to examine the integration of thresholding methods with other techniques, such as machine learning or object-based image analysis, to further explore accuracy improvements under various image conditions.

References

Amansya, I., Indra, J., Nurlaelasari, E., & Juwita, A. R. (2024). Prediksi penjualan kendaraan menggunakan regresi linear: Studi kasus pada industri otomotif di indonesia. *Innovative: Journal of Social Science Research*, *4*(4), 1199–1216

Andini, S. W., Prasetyo, Y., & Sukmono, A. (2018). Analisis sebaran vegetasi dengan citra satelit sentinel menggunakan metode NDVI dan segmentasi. *Jurnal Geodesi Undip*, *7*(1), 14–24.

Arianto, M. F. (2020). Potensi wilayah pesisir di negara Indonesia. *Jurnal Geografi*, *10*(1), 204–215.

Aryastana, P., Eryani, I. G. A. P., & Candrayana, K. W. (2016). Perubahan garis pantai dengan citra satelit di Kabupaten Gianyar. *PADURAKSA: Jurnal Teknik Sipil Universitas Warmadewa*, *5*(2), 70–81. https://doi.org/10.22225/pd.5.2.379.70-81

Botev, Z. I., Grotowski, J. F., & Kroese, D. P. (2010). Kernel density estimation via diffusion. Annals of Statistics, 38(5), 2916–2957.

Chicco, D., Warrens, M. J., & Jurman, G. (2021). The coefficient of determination R^2 is more informative than SMAPE, MAE, MAPE, MSE and RMSE in regression analysis evaluation. *PeerJ Computer Science*, *7*, e623.

Dey, M., Bhardwaj, V. K., & Jena, B. K. (2024). Half-a-century (1972-2022) of shoreline dynamics and forecast with responsible driving forces in West Bengal Coast: A remote sensing and statistical approach. *SSRN*. https://doi.org/10.2139/ssrn.4933055

Diasa, I. W., Semarabawa, I. G. A. B., & Sukawati, N. K. S. A. (2024). Analisis desain revetment batu armor dalam penanggulangan kerusakan pantai Tegal Besar di Kabupaten Klungkung. *Jurnal Ilmiah Vastuwidya*, *7*(1), 15–26.

Du, Y., Zhang, Y., Ling, F., Wang, Q., Li, W., & Li, X. (2016). Water bodies' mapping from Sentinel-2 imagery with modified normalized difference water index at 10-m spatial resolution produced by sharpening the SWIR band. *Remote Sensing*, *8*(4), 354.

Esendağlı, Ç., Selim, S. E. R. D. A. R., & Demir, N. U. S. R. E. T. Comparison of shoreline extraction indexes performance using Landsat 9 satellite images in the heterogeneous coastal area. *[Nama Jurnal Tidak Tersedia]*.

Feyisa, G. L., Meilby, H., Fensholt, R., & Proud, S. R. (2014). Automated Water Extraction Index: A new technique for surface water mapping using Landsat imagery. *Remote Sensing of Environment*, *140*, 23–35.

Hassan, Q. K., Doxee, A., & Gillis, D. J. (2018). Improving shoreline mapping from remote sensing imagery using smoothing techniques. *Remote Sensing Applications: Society and Environment*, *10*, 102–112.

Hastuti, A. W., Ismail, N. P., & Nagai, M. (2024). Analysis of coastline extraction indices using Sentinel-2 and Google Earth Engine, case study in Bali, Indonesia. In *BIO Web of Conferences* (Vol. 106, p. 04004). EDP Sciences.

Hidayah, R. T. N., Putra, R. D., Jaya, Y. V., & Suhana, M. P. (2018). Pola perubahan garis pantai di Pulau Dompak periode 2005-2015. *Dinamika Maritim*, *7*(1), 15–19.

Kannan, R., Ramanamurthy, M. V., & Kanungo, A. (2016). Shoreline change monitoring in Nellore coast at east coast Andhra Pradesh District using remote sensing and GIS. *Journal of Fisheries and Livestock Production*, *4*(4), 161. https://doi.org/10.4172/2332-2608.1000161

Kilibarda, Z., Graves, N., Dorton, M., & Dorton, R. (2014). Changes in beach gravel lithology caused by anthropogenic activities along the southern coast of Lake Michigan, USA. *Environmental Earth Sciences*, *71*, 1249–1266. https://doi.org/10.1007/s12665-013-2529-2

Korneev, S., Gilles, J., & Battiato, I. (2022). Multiclass histogram-based thresholding using kernel density estimation and scale-space representations. arXiv preprint arXiv:2202.04785.

Li, J., & Chen, W. (2021). Variational-scale segmentation for multispectral remote-sensing images. *Remote Sensing*, *14*(2), 326.

Li, J., & Roy, D. P. (2017). A global analysis of Sentinel-2A, Sentinel-2B and Landsat-8 data revisit intervals and implications for terrestrial monitoring. *Remote Sensing*, *9*(9), 902.

Li, W., & Gong, P. (2016). Continuous monitoring of coastline dynamics in western Florida with a 30-year time series of Landsat imagery. *Remote Sensing of Environment*, *179*, 196–209.

Linton, N. (2017, Maret 29). *Otsu's method for image segmentation*. Medium.

Liu, S., Wu, Y., Zhang, G., Lin, N., & Liu, Z. (2023). Comparing water indices for Landsat data for automated surface water body extraction under complex ground background: A case study in Jilin Province. *Remote Sensing*, *15*(6), 1678.

Micallef, S., Micallef, A., & Galdies, C. (2018). Application of the Coastal Hazard Wheel to assess erosion on the Maltese coast. *Ocean & Coastal Management*, *156*, 209–222. https://doi.org/10.1016/j.ocecoaman.2017.06.005

Otsu, N. (1979). A threshold selection method from gray-level histograms. IEEE Transactions on Systems, Man, and Cybernetics, 9(1), 62–66.

Pahlevan, N., Mangin, A., Balasubramanian, S. V., Smith, S. M., Al-Hamdan, M. Z., Schalles, J., Duforet, L., Ruddick, K. G., Li, R. R., & Franz, B. A. (2017). Sentinel-2 MultiSpectral Instrument (MSI) data processing for aquatic science applications: Demonstrations and validations. *Remote Sensing of Environment*, *201*, 47–56.

Parenta, J. (2021). *Analisis perubahan garis pantai Kabupaten Maros menggunakan teknologi penginderaan jauh* [Skripsi, Universitas Hasanuddin].

Pham, T. D., Le, T. H., Niyogi, A., & Pham, M. T. (2019). Remote sensing approaches for monitoring mangrove species, structure, and biomass. *Remote Sensing*, *11*(3), 230.

Ranasinghe, R. (2016). Assessing climate change impacts on open sandy coasts: A review. *Earth-Science Reviews*, *160*, 320–332. https://doi.org/10.1016/j.earscirev.2016.07.011

Safitri, F., Suryanti, & Febrianto, S. (2019). Analisis perubahan garis pantai akibat erosi di pesisir Kota Semarang. *Jurnal Ilmiah Geommatika*, *25*(1), 37–46.

Singa, J. C. B. G., Nuarsa, I. W., & Putra, I. G. N. (2023). Deteksi perubahan garis pantai menggunakan citra satelit Sentinel-2 di Kabupaten Klungkung, Bali. *Journal of Marine and Aquatic Sciences*, *9*(1), 70–81.

Suryanto, A. A., & Muqtadir, A. (2019). Penerapan metode mean absolute error (MEA) dalam algoritma regresi linear untuk prediksi produksi padi. *Saintekbu*, *11*(1), 78–83.

Tang, W., Zhao, C., Lin, J., et al. (2022). Improved Spectral Water Index Combined with Otsu Algorithm to Extract Muddy Coastline Data. Water, 14(6), 855.

Toure, S., Diop, O., Kpalma, K., & Maiga, A. S. (2019). Shoreline detection using optical remote sensing: A review. *ISPRS International Journal of Geo-Information*, *8*(2), 75.